Advanced Composites and Hybrid Materials (2021) 4:591–601
https://doi.org/10.1007/s42114-021-00275-4

ORIGINAL RESEARCH

Study on broadband microwave absorbing performance of gradient porous structure

Feng Luo[1] · Dongqing Liu[2] · Taishan Cao[1] · Haifeng Cheng[2] · Jiacai Kuang[1,3] · Yingjun Deng[1,3] · Wei Xie[1,2,3]

Received: 12 March 2021 / Revised: 9 May 2021 / Accepted: 13 May 2021 / Published online: 18 June 2021

Abstract

In this study, a gradient porous structure was designed for a novel microwave absorbing material, and the effects of various factors on its microwave absorbing characteristics were investigated. The computational and experimental results show that the bandwidth of this composite can reach up to 14.06 GHz with a microwave reflection loss below − 10 dB in the frequency of 1–18 GHz. The appreciable agreement between the simulation and the experiment verified the validity of this structure. The broadband microwave absorbing performance of designed gradient porous structure was significantly enhanced, which was ascribed to the synergistic effect of structural and material characteristics. The square aperture of this structure increased from the bottom to the top, which improved the impedance matching between the surface of gradient porous structure and the air and reduced the reflection of electromagnetic waves. In addition, the transmission path of electromagnetic wave inside the absorbing structure increased, thus facilitating the attenuation of electromagnetic wave. This study could provide a new design strategy for the research of antiradar detection technique and shielding the electromagnetic interference.

Keywords Radar absorbing structure · Broadband absorption · 3D printing · Gradient porous structure

1 Introduction

The stealth technique is a comprehensive technique that reduces the scattering cross section of the target radar to make it difficult to be detected, identified, and hit within a certain range. To scatter and absorb the incident electromagnetic wave is a fundamental way for microwave-absorbing materials to achieve the stealth of radar. Different excellent absorbents have been developed, such as carbon fiber and carbon nanotube [1–3], silicon carbide [4, 5], carbon-based composite materials [3, 6, 7], ferrite [8], magnetic metal powder [9], and MXenes [10, 11]. However, with the continuous development and popularization of advanced optoelectronics, radar detection, and guidance techniques, the threat frequency bands for weapons and equipment have been expanded to the decimeter, and centimeter and millimeter wave bands of L(1–2 GHz), S(2–4 GHz), C(4–8 GHz), X(8–12 GHz), Ku(12–18 GHz), and Ka(26.5–40 GHz). The requirements for the microwave absorbing materials with broad band, strong absorption, thin thickness, and low density have been continuously improved [12–16]. It is not enough for microwave-absorbing materials to meet the requirements of current antiradar detection technique. Therefore, most researches have focused on the combination of structural design and materials characteristics for multifunctional integration, which was also applied to aeronautical engineering. Results show that the combination of structural design and materials characteristics is an effective way to obtain excellent broadband microwave-absorbing materials.

At present, many studies on radar absorbing structures are based on the synergy of materials and structures, such as honeycomb structure [17–19], pyramid structure [20], laminated structure [21–23], cycle structure [24–28], and metamaterials [29, 30]. These studies have achieved the best

✉ Feng Luo
291697097@qq.com

✉ Wei Xie
xwxw00@163.com

[1] School of Automotive and Mechanical Engineering, Changsha University of Science & Technology, Hunan 410114, China

[2] Science and Technology On Advanced Ceramic Fibers and Composites Laboratory, National University of Defense Technology, Hunan 410073, China

[3] Hunan Provincial Key Laboratory of Flexible Electronic Materials Genome Engineering, Changsha University of Science & Technology, Hunan 410114, China

absorbing effect by using different materials and adjusting the structural parameters, but it is still difficult for these radar-absorbing structures to achieve an absorption rate of more than 90% at 1–18 GHz. The main reason is that a huge impedance mismatch between the radar absorbing structures and the free space is generated, resulting in massive reflected electromagnetic waves. Therefore, the design of new structures with broadband absorbing effect is still one of the current research hotspots. It is shown that the design of porous structure can not only reduce the weight of microwave-absorbing composites, but also alleviate the impedance mismatch and enhance the multiple scattering absorption in the pores. Furthermore, developing multilayer composite through the gradient structure can also lower the impedance mismatch and solve the problem of narrow band currently.

In this study, a gradient porous structure (GPS) was designed for broadband microwave–absorbing material, which reduced the reflection of electromagnetic waves by adjusting the impedance matching. In addition, with the decrease of square aperture, the contact area between microwave absorbing materials and electromagnetic wave increased to extend the transmission path of electromagnetic wave in the absorbing structure and increase the attenuation loss, thus achieving the broadband-absorbing effect. The effect of geometric parameters and conductivity of GPS on the absorbing performance was simulated through the CST Microware Studio, and the GPS was prepared by 3D printing techniques and impregnation method to verify the simulation results. This structure could provide a reference for the design and preparation of broadband microwave–absorbing materials.

2 Structural design and simulation process

2.1 Structural design strategy

Excellent microwave = absorbing material should meet the following requirements: (1) The impedance of material (Z_0) should match with the optimal impedance of air ($Z_{air} = 377\ \Omega$) as much as possible. The input impedance of general absorbing material is calculated by Eq. (1). (2) The electromagnetic waves should be able to decay rapidly when entering the microwave-absorbing materials. In this study, the radar absorbing structure can rapidly attenuate the electromagnetic wave and redesign the impedance to match with that of air.

$$Z_0 = Z_{air}\sqrt{\frac{\mu}{\varepsilon}}\tanh\left[j\left(\frac{2\pi df}{c}\right)\sqrt{\frac{\mu}{\varepsilon}}\right] \tag{1}$$

The structure diagram of GPS is shown in Fig. 1. Based on the square aperture of the bottom layer, the square structure was divided into multiple layers, and the square aperture of each layer above is bigger than that of its bottom layer. The excellent absorbing performance of GPS is resulted from the combination of structure and conductive layer. As the square aperture of upper layer of structure was enlarged, the contact area between the upper layer and the air was larger. When the electromagnetic waves were emitted from the upper layer of structure, the reflection was reduced so that more electromagnetic waves can enter the bottom layer of structure. In the process of electromagnetic waves entering the bottom layer of the

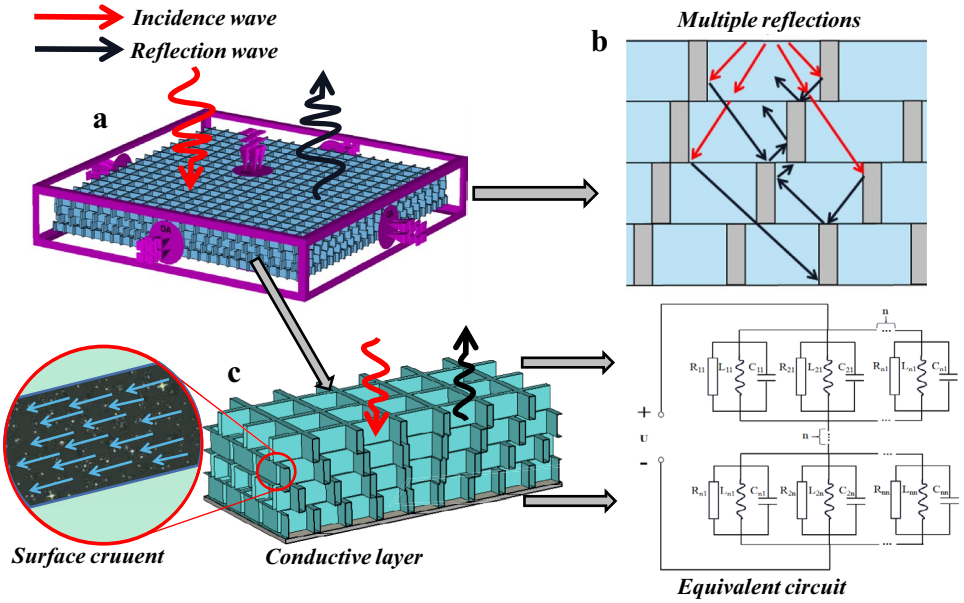

Fig. 1 Schematic diagram of radar absorbing mechanism of GPS

structure, as the square aperture of holes became smaller, the contact area between the electromagnetic waves and the conductive layer increased so that the conductive layer absorbed more electromagnetic waves. Moreover, some reflected electromagnetic waves contacted with the conductive layer again within the structure and were absorbed twice or more times. The electromagnetic wave absorbing process of GPS is shown in Fig. 1b. The reflected waves were also reflected and refracted multiple times in the gaps of structure, thus increasing the wastage of electromagnetic waves inside the structure, which achieved an excellent absorbing effect.

As shown in Fig. 1c, according to the electromagnetic induction theory, electromagnetic waves caused the conductive layer to form surface current during the incident process, and the current flowed from the top to the bottom along the conductive layer to form a loop, that is, the equivalent circuit. Therefore, the incident electromagnetic wave energy was also lost. Under the action of electromotive force, free electrons moved directionally. When the overall impedance of structure was close to that of electromotive force, an excellent impedance matching was formed. In this impedance matching, the GPS obtained excellent electromagnetic wave absorbing performance. The impedance of GPS was represented by the equivalent circuit composed of capacitance (C), inductance (L), and resistance (R). As shown in Eq. (2), Z_1 was represented by a combination of RCL in which the capacitance and inductance correspond to the geometric structures, and the resistance was determined by the surface resistance of material. Therefore, in order to achieve excellent impedance matching, the geometric structures and surface resistance were changed to adjust the impedance of structure.

$$Z_1 = R - jX = R - j\left(\frac{1}{\omega C} - \omega L\right) \tag{2}$$

Based on these analyses, it can be inferred that the electromagnetic wave–absorbing performance of GPS is determined by the impedance and the shape of structure and affected by the changes of interfacial resonance and polarization. Therefore, better impedance matching can be obtained by optimizing the surface resistance and geometric size. Because of the geometric structure, the GPS contains a variety of losses, including the reflection loss between the gaps, the microstructure loss of material, and the electromagnetic effect between square holes, which can rapidly attenuate the electromagnetic waves entering the conductive layer. Therefore, by optimizing the impedance matching, the GPS can have excellent broadband absorbing performance.

2.2 Model design and simulation

Figure 2 is a schematic diagram of GPS, which is composed of periodic square holes stacked. The total height of structure is H, and the height of each layer is $h = H/$(number of layers). The apertures of square holes from the bottom to the top are l_1, l_2, l_3, and l_4 respectively. The wall thickness is w, and the material surface resistance is R.

In the simulation process, a finite element integral technique (CST Microwave Studio) was used. The parameters were set as follows: the frequency range is 1–18 GHz. The electromagnetic wave is perpendicular to the Z-axis and emitted from the positive direction of Z-axis in the form of plane wave. The direction H of magnetic field is perpendicular to that of electric field. The calculation formula of absorbing rate is $A(\omega) = 1 - T(\omega) - R(\omega)$, [$R(\omega) = |S_{11}|^2$, $T(\omega) = |S_{21}|^2$]. According to frequency, the transmittance and reflectance can be derived by parameter S respectively. Since the back surface is in contact with the metal surface during the testing and simulation, the transmittance $T(\omega)$ in the calculation formula is 0. Therefore, the absorbing rate was expressed as $A(\omega) = 1\text{-}R(\omega)$.

3 Results and discussion

3.1 Selection of square aperture and number of layers

Through the simulation of different apertures of single-layer square hole structure, the square aperture at the bottom layer with the best effect was selected in this study. The test results are shown in Fig. 3a; under the conditions of $H = 20$ mm, $w = 0.5$ mm, and $R = 500$ Ω/sq, the absorbing effect of single-layer square hole structure becomes better and better as the square aperture increases. It reaches the best when $l = 6$ mm and becomes worse and worse when the square aperture continues to increase. Therefore, the square aperture of 6 mm at the bottom layer was selected, which is gradually expanded from the bottom to the top, that is, starting from the bottom layer, the square apertures are $l_1 = 6$ mm, $l_2 = 7$ mm, $l_3 = 8$ mm, and $l_4 = 9$ mm, respectively.

Then, structures of different layers with the same wall thickness, surface resistance, and height were compared, as shown in Fig. 3b. Under the conditions of $w = 0.5$ mm, $R = 500$ Ω/sq, and $H = 20$ mm, when the number of structural layers with the same wall thickness, surface resistance, and height increases, the trend of reflection loss curve is relatively close. There are two peaks at 2–4 GHz and 10–12 GHz. The absorbing effect at 1–2 GHz is very close, but is greatly improved at 2–18 GHz. The improvement

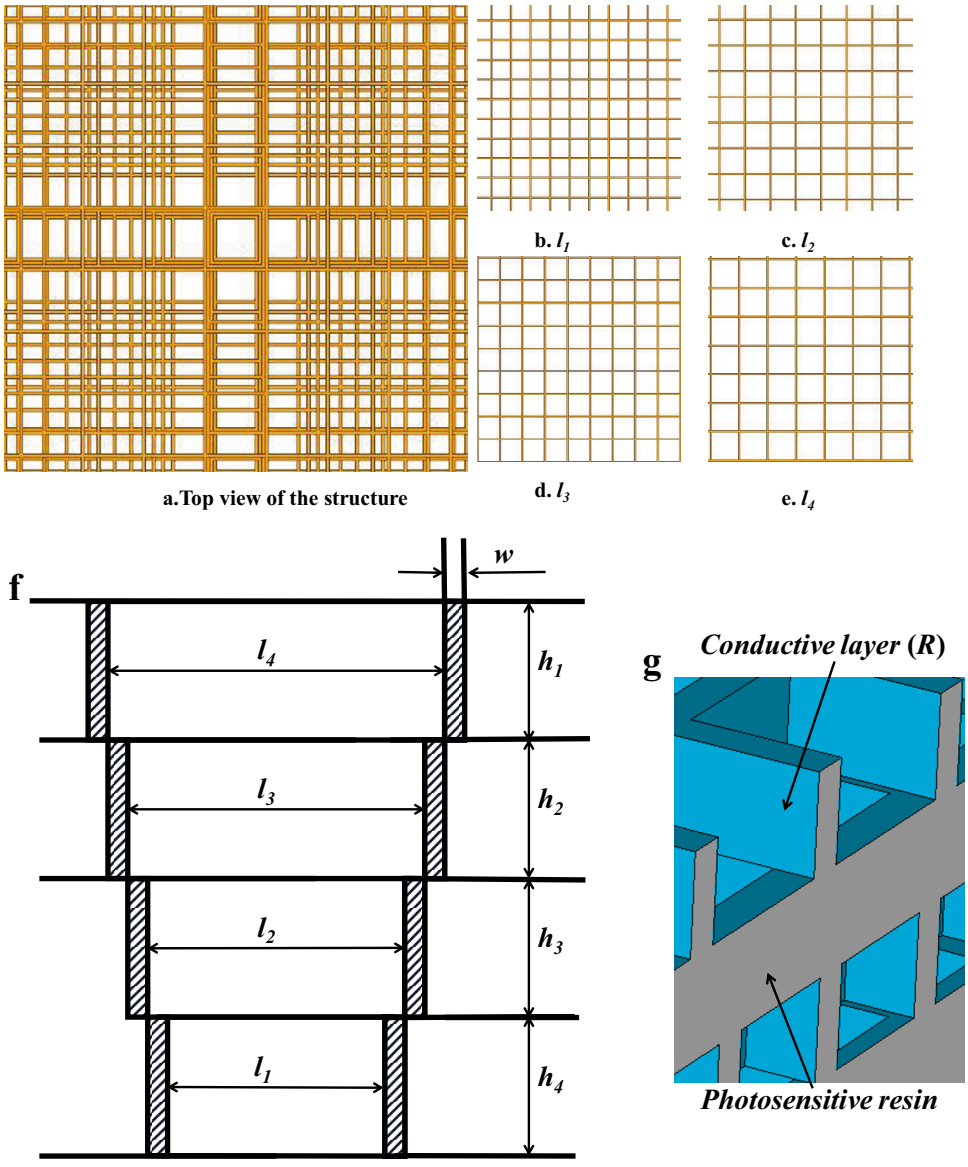

Fig. 2 Schematic diagram of GPS

effects of two-layer and three-layer are relatively close. The absorbing effect of four-layer is the best. As a result, the GPS with four layers was selected.

Detailed simulation parameters of GPS are shown in Table 1.

3.2 Radar absorbing characteristics

Through the simulation analysis of different surface resistances of structure, Fig. 4a shows the effect of different surface resistances on the reflection loss under the conditions of four layers, $H = 20$ mm and $w = 1.0$ mm. It can be seen from the diagram that with the increase of surface resistance, three peaks gradually appear in the reflection loss curve at 3–4 GHz, 9–10 GHz, and 15–16 GHz, respectively. In the interval, the reflection loss reaches the maximum. When the surface resistance is 1000 Ω/sq, the reflection loss of three peaks is the maximum, that is, − 39.7 dB, − 31.1 dB, and − 45.3 dB, respectively. As the surface resistance continues to increase, it gradually decreases. Therefore, the reflectance curve becomes smoother.

Only increasing the height of structure, the overall variation rule of reflectance curve is basically same, but the peak of reflectance curve moves toward the low frequency as H increases. As shown in Fig. 4c, under the conditions of four layers, $w = 1$ mm and $R = 1500$ Ω/sq, the first peak moves from 5 GHz ($H = 14$ mm) to 3 GHz ($H = 26$ mm), and its reflection loss curve gradually increases. As the absorbing peak moves toward the low frequency, the absorbing performance of GPS in each frequency band becomes better and better. Therefore, the higher the H, the better the absorbing performance of structure.

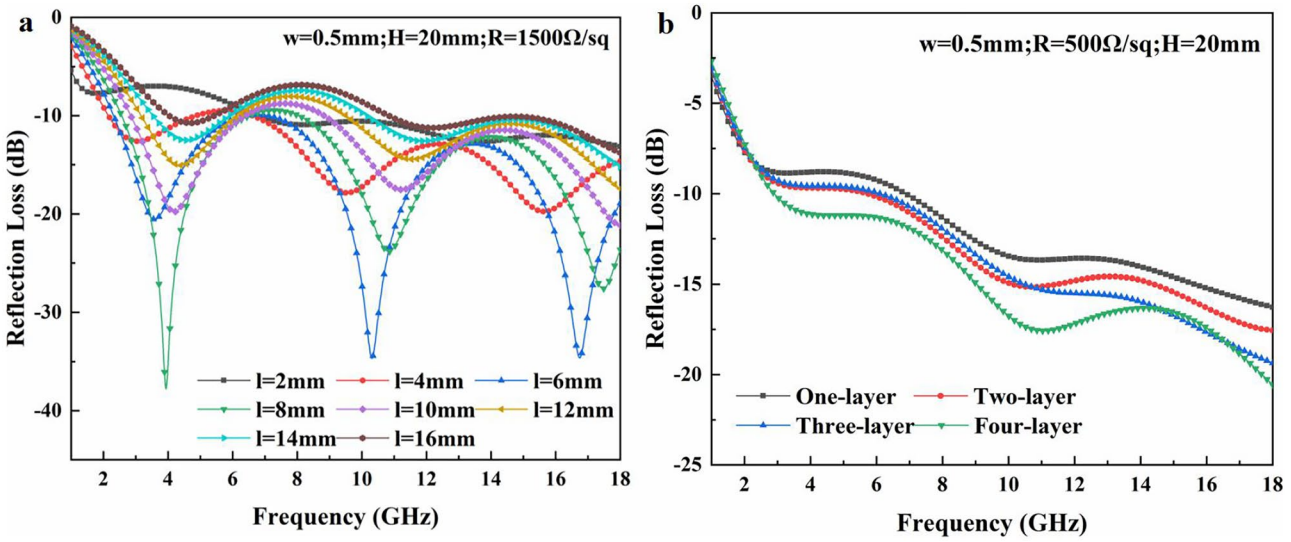

Fig. 3 **a** Comparison of different square apertures, **b** comparison of different layers

Under the conditions of four layers, $R = 1000$ Ω/sq and $H = 20$ mm, the effect of different wall thicknesses on the reflection loss is shown in Fig. 4b. Increasing the wall thickness makes all loss peaks move toward the low frequency, which has better absorbing effect in the low-frequency band. However, as the wall thickness increases, the peak of reflection loss curve moves to the low frequency, while the loss value of some bands decreases on the contrary. For example, when the wall thickness w is 0.4 mm, the loss value of 4–8 GHz is lower than − 10 dB. However, when the wall thickness w increases to 1.6 mm, the loss value of some bands of 4–8 GHz is higher than − 10 dB.

The effect of wall thickness on the absorbing performance of structure cannot be distinguished only from the reflection loss curve. As a result, the bandwidth below − 10 dB with different R, w, and H was compared. As shown in Fig. 4d, when the surface resistance is small, the difference in wall thickness has little influence on the bandwidth below − 10 dB, which is very close. However, when the surface resistance is large, the bandwidth below − 10 dB decreases significantly with the increase of wall thickness. Therefore, it is concluded that when the wall thickness is smaller, the absorbing performance of structure is better. From the comparison of bandwidth below − 10 dB with

Table 1 Parameters of GPS

Parameters	Expressions	Variables	Invariants
R	Sheet resistance/ Ω/sq	200, 400, 500, 600, 800, 1000, 1200, 1400, 1500, 1600, 1800, 2000	$N=4$; $w=1$, 1.5, 2 mm; $H=18$, 20, 22 mm; $h=4.5$, 5, 5.5 mm; $l_1=6$ mm; $l_2=7$ mm; $l_3=8$ mm; $l_4=9$ mm
N	Number of layers	4, 3, 2, 1	$R=500$ Ω/sq; $w=0.5$ mm; $l_1=6$ mm; $l_2=7$ mm; $l_3=8$ mm; $l_4=9$ mm; $H=20$ mm
w	Thickness of wall/mm	0.4, 0.5, 0.6, 0.8, 1.0, 1.2, 1.4, 1.5, 1.6, 1.8, 2.0	$N=4$; $H=20$ mm; $R=1000$ Ω/sq; $l_1=6$ mm; $l_2=7$ mm; $l_3=8$ mm; $l_4=9$ mm
l	Aperture of square hole/mm	2, 4, 6, 8, 10, 12, 14, 16	$N=1$; $H=20$ mm; $w=0.5$ mm; $R=1500$Ω/sq
H	Total thickness/mm	14, 16, 18, 20, 22, 24, 26	$N=4$; w = 1.0 m; $R=1500$ Ω/sq; $l_1=6$ mm; $l_2=7$ mm; $l_3=8$ mm; $l_4=9$ mm;
h	Height of single layer/mm	H/N	/

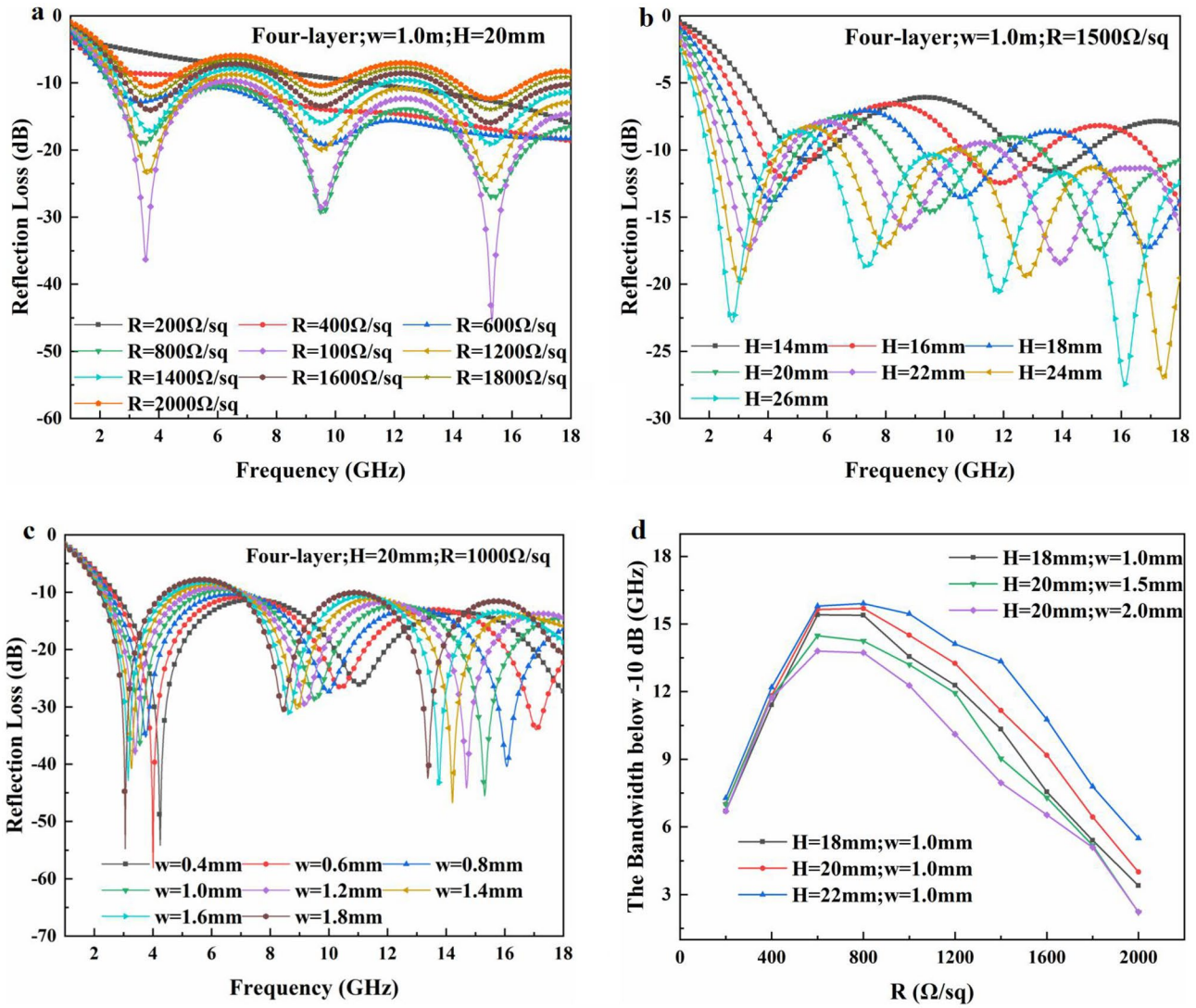

Fig. 4 **a** Effect of surface resistance *R* on the reflection loss curve, **b** effect of height *H* on the reflection loss curve, **c** effect of wall thickness *w* on the reflection loss curve, **d** effect of *R*, *w*, and *H* on the bandwidth below – 10 dB for four-layer structure

different surface resistances and heights, it can be seen that when the surface resistance increases, the bandwidth also increases. When the surface resistance is 800 Ω/sq, the bandwidth reaches the maximum. When the surface resistance continues to increase, the bandwidth below – 10 dB gradually decreases. Therefore, when the surface resistance is 800 Ω/sq, the structure has the best microwave-absorbing performance. In addition, increasing the height is conducive to the absorbing performance of structure.

3.3 Experimental verification

Based on the above analysis, it is concluded that when *w* decreases and *H* increases, the absorbing performance is better. When the surface resistance is 800 Ω/sq, the absorbing performance reaches the best. However, increasing or decreasing the surface resistance makes the absorbing performance worse. Table 2 shows the comparison of various parameters below – 10 dB bandwidth:

If *w* is too small, it makes the preparation of sample difficult. In practical applications, *H* should be as small as possible when the conditions are met. Thus, values of parameters used for verification in this study are shown in Table 3.

In order to verify the reliability of design, the GPS was prepared by 3D printing techniques and impregnation method to compare the simulation results. All the materials needed in the experiment can be bought in merchants and used without processing. Firstly, a photosensitive resin was used to prepare a structured matrix by light curing. Secondly, graphite (180 g), conductive carbon black (35 g), dispersant (20 g), curing agent (50 g), and water (300 g) were added to the water-based epoxy resin (550 g). Thirdly, the

Table 2 Comparison of various parameters with bandwidths below − 10 dB

Parameters	Variables	Invariants	Absorbing peaks (GHz)	Peak values (dB)	Bandwidths below − 10 dB (GHz)
H	14 mm	W = 1 mm; N = 4; R = 1000 Ω/sq; l_1 = 6 mm; l_2 = 7 mm; l_3 = 8 mm; l_4 = 9 mm	5.23; 13.63	− 19.37; − 19.47	11.69
	16 mm		4.52; 11.95	− 23.95; − 21.58	12.33
	18 mm		3.99; 10.61; 16.99	− 33.35; − 24.59; − 40.27	13.55
	20 mm		3.57; 9.55; 15.31	− 36.35; − 28.73; − 45.52	14.50
	22 mm		3.21; 8.68; 13.97	− 26.28; − 36.26; − 49.64	15.45
	24 mm		2.90; 7.97; 12.83; 17.42	− 22.04; − 47.15; − 37.38; − 26.71	16.06
	26 mm		2.67; 7.36; 11.86; 16.18	− 19.46; − 33.19; − 32.69; − 25.69	16.23
w	0.4 mm	N = 4; H = 20 mm; R = 500 Ω/sq; l_1 = 6 mm; l_2 = 7 mm; l_3 = 8 mm; l_4 = 9 mm	11.42	− 17.71	15.01
	0.6 mm		10.76	− 17.43	15.18
	0.8 mm		10.38	− 16.88	15.19
	1.0 mm		9.82	− 16.34	15.23
	1.2 mm		3.22; 9.39; 16.41	− 10.59; − 15.88; − 18.47	14.01
	1.4 mm		3.06; 9.02; 15.99	− 10.62; − 15.53; − 19.41	13.53
	1.6 mm		2.97; 8.72; 13.92	− 10.58; − 15.17; − 17.36	13.20
	1.8 mm		2.82; 8.44; 13.51	− 10.68; − 15.00; − 16.88	13.14
R	400 Ω/sq	*N* = 4; *H* = 20 mm; *w* = 1.0 mm; l_1 = 6 mm; l_2 = 7 mm; l_3 = 8 mm; l_4 = 9 mm	–	–	11.82
	600 Ω/sq		3.40; 9.7	− 12.82; − 19.19	15.64
	800 Ω/sq		3.48; 9.57; 15.37	− 19.02; − 29.42; − 27.09	15.69
	1000 Ω/sq		3.57; 9.55; 15.31	− 36.35; − 28.73; − 45.52	14.50
	1200 Ω/sq		3.62; 9.55; 15.28	− 23.53; − 19.94; − 24.39	13.25
	1400 Ω/sq		3.67; 9.53; 15.28	− 17.22; − 15.93; − 19.08	11.16
	1600 Ω/sq		3.70; 9.53; 15.25	− 14.06; − 13.48; − 15.93	9.18
	1800 Ω/sq		3.73; 9.53; 15.25	− 12.03; − 11.74; − 13.95	6.44
N	1	*H* = 20 mm; *w* = 0.5 m; *R* = 500 Ω/sq; l_1 = 6 mm; l_2 = 7 mm; l_3 = 8 mm; l_4 = 9 mm	10.93	− 13.69	11.12
	2		10.72	− 15.15	12.31
	3		–	–	11.90
	4		9.82	− 16.34	15.30

substrate of porous gradual structure was immersed in the conductive paint. It was taken out 1 min later and placed in an oven to dry for 12 h at 40 °C. A conductive layer was then formed on the surface of substrate of porous gradual structure. Finally, the surface resistance of structure was tested by a four-probe tester and an arch reflectivity test system (8720ES, Agilent, USA) to measure the reflection loss in a microwave darkroom. The antenna type is a segmented pyramid horn antenna, and the distance from the metal plate is about 1.8 m.

The comparison between test results and simulation results is shown in Fig. 5c, d. It is found that the test results basically conform to the simulation results. However, there is also a certain difference between the test and the

Table 3 Values of parameters for verification

Samples	Value of R (Ω/sq)	Value of w (mm)	Value of H (mm)
Measured 1	400	1	20
Measured 2	400	2	20
Measured 3	800	1	20
Measured 4	2000	1	20

simulation, which is caused by the following reasons: (1) The coating of sample in the test is thicker than that in the simulation. (2) The coating is uneven during the preparation process. (3) The specific value of resistance inside the structure cannot be measured, including the average value of resistance. (4) Compared with the vertical incidence of electromagnetic waves in the simulation, there are some angular deviations between the antenna and the sample in the test, and the test results of 1–18 GHz are composed of four frequency bands of 1–2 GHz, 2–4 GHz, 4–8 GHz, and 8–18 GHz. These four frequency bands with four different antennas changed the antenna during the test and caused position deviation. Therefore, these factors caused certain errors in this test. Considering the uncertainty in preparation and test, there is a certain error between the simulation and the test, but it still has a certain reference. In the test results, under the conditions of $H = 20$ mm, $w = 1$ mm, and $R = 800$ Ω/sq, the bandwidth of reflectivity curve below − 10 dB is 14.06 GHz (3.98–18 GHz). At 5.34 GHz, the value of reflection loss can reach − 17.46 dB.

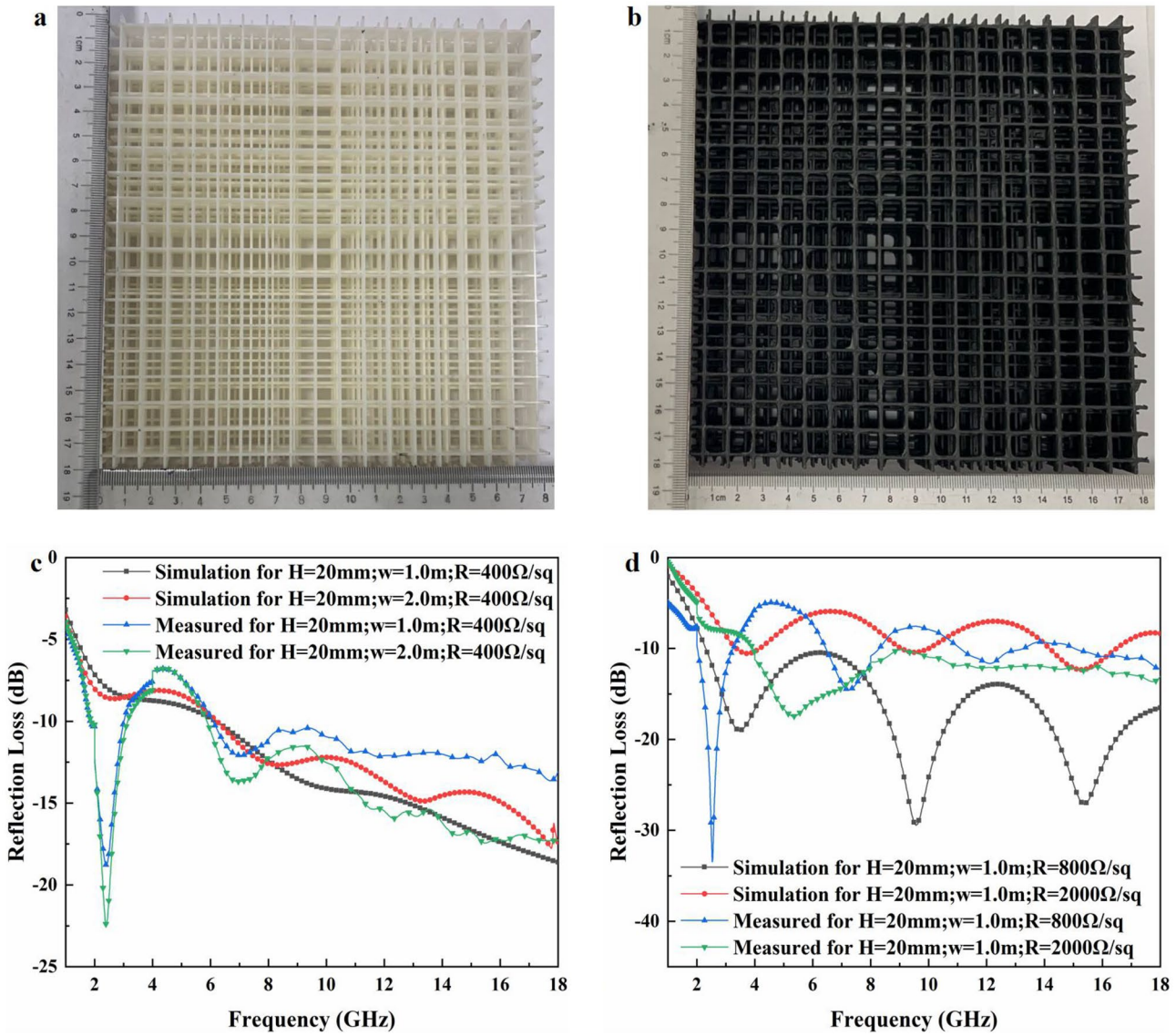

Fig. 5 **a** GPS matrix, **b** GPS impregnated with conductive coating, **c** simulated and measured RL with different values of *w*, **d** simulated and measured RL with different values of *R*

According to the simulation results, under the conditions of $H = 20$ mm, $w = 1$ mm, and $R = 800$ Ω/sq, the reflectance curve has three peaks at 3.48 GHz, 9.57 GHz, and 15.38 GHz, respectively. Figure 6 is a schematic diagram of magnetic field distribution and surface current of three peaks and one other-than-peaks during the simulation. It can be seen from the figure that when the frequency is 3.48 GHz, the magnetic field strength near the upper and bottom metal of the square hole structure is higher, and the magnetic field strength in other places is weaker, which is mainly concentrated on the top and the bottom. Without peak, when the frequency is 8.0 GHz, the intensity of the magnetic field inside the structure is the highest. The distribution of magnetic field at 9.57 GHz is consistent with that at 8.0 GHz. When the frequency is 15.38 GHz, it is only concentrated on the top of the structure, indicating that the magnetic field has been changing from the beginning to the end. The intensity of generated surface current also changes, which is thus consistent with the intensity of the magnetic field. A typical λ/4 resonance is shown, that is, the electromotive force exerted by the incident electromagnetic wave excites the magnetic field inside the porous structure, and

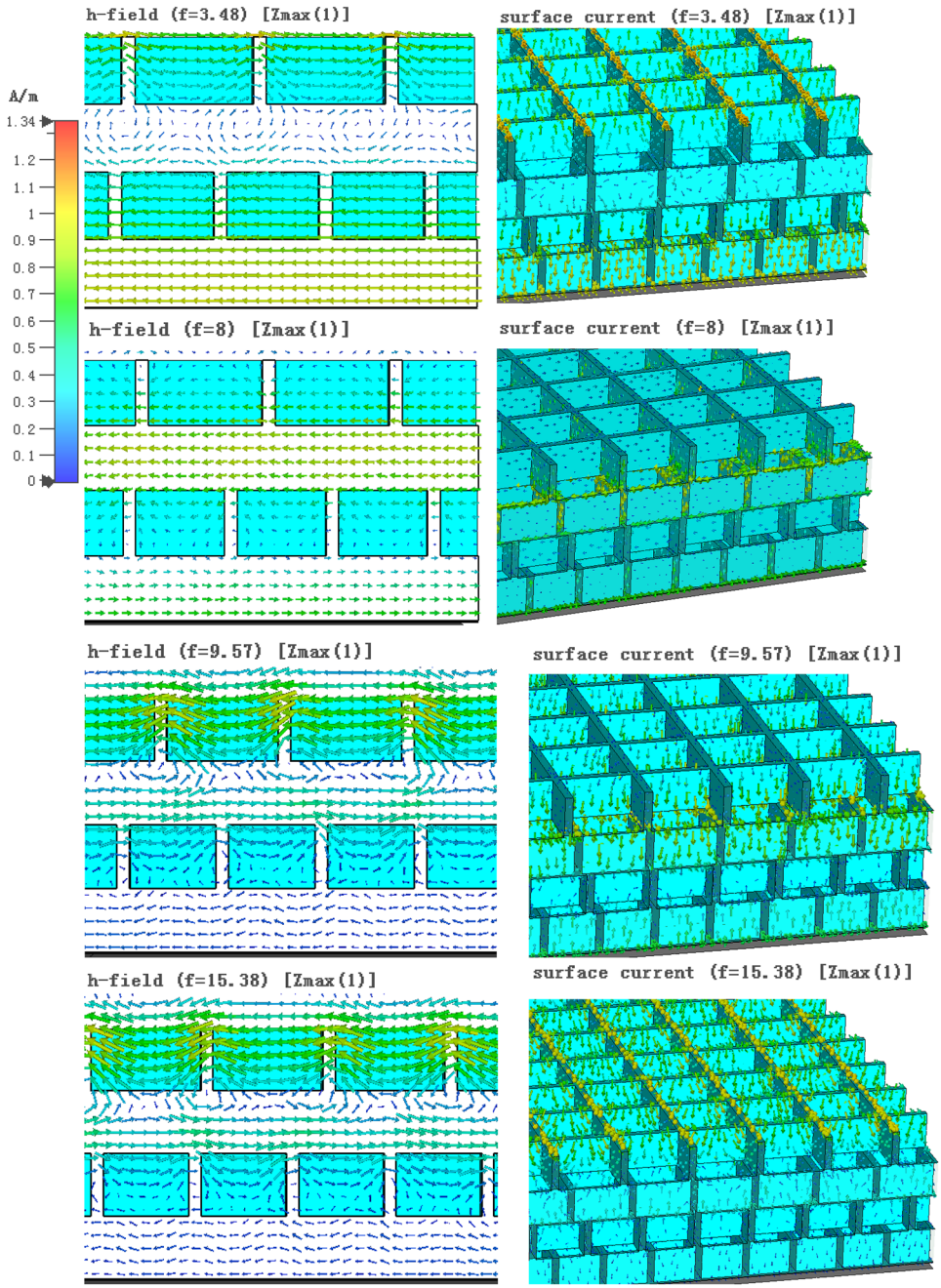

Fig. 6 Schematic diagram of magnetic field distribution and surface current

then generates the resonance near the resonant medium of conductive layer of structure, thereby changing the dielectric constant. It also resonates the reflectivity curve of GPS and changes the absorbing bandwidth. Therefore, when it has a suitable surface resistance value, the conductive layer can make more electromagnetic waves enter the structure and more attenuated. This is consistent with our conjecture. As a result, the GPS is effective.

4 Conclusions

In summary, the designed and prepared gradient porous composites with three-dimensional structure and conductive coating display an excellent electromagnetic wave–absorbing performance, which is attributed to the synergistic effect of structure and material. The impedance of GPS is affected by the surface resistance R, the total height H, and the wall thickness w. By optimizing R, H, and w, the structure can achieve good impedance matching with the air, thereby obtaining excellent absorbing performance. Under the conditions of $H = 20$ mm, $w = 1$ mm, and $R = 800$ Ω/sq, the prepared GPS can reach 14.06 GHz with the bandwidth below − 10 dB. It is shown that the GPS prepared by 3D printing techniques and impregnation method has obvious consistency with the simulation results, which proves the validity of theory in this study. Therefore, a GPS proposed in this study can effectively improve the absorbing performance. This study can also provide a new technical approach for developing "thin, light, wide, strong" radar stealth materials.

Supplementary information The online version contains supplementary material available at https://doi.org/10.1007/s42114-021-00275-4.

Funding This work is financially supported by the National Natural Science Foundation of China (Grant 61871060, 51201022), the project of Science and Technology on Advanced Ceramic Fibers and Composites Laboratory (WDZC20195500502), and Changsha Science and Technology Project (kq2004069).

Declarations

Conflict of interest The authors declare no competing interests.

References

1. Cao M, Song W, Hou Z, Wen B, Yuan J (2010) The effects of temperature and frequency on the dielectric properties, electromagnetic interference shielding and microwave-absorption of short carbon fiber/silica composites. Carbon 48:788–796
2. Zhao B, Li Y, Guo XQ, Zhang R, Zhang JX, Hou H, Ding T, Fan JC, Guo ZH (2019) Enhanced electromagnetic wave absorbing nickel (oxide)-carbon nanocomposites. Ceram Int 45:24474–24486
3. Micheli D, Apollo C, Pastore R, Marchetti M (2010) X-band microwave characterization of carbon-based nanocomposite material, absorption capability comparison and RAS design simulation. Compos Sci Technol 70:400–409
4. Li W, Li C, Lin L, Wang Y, Zhang J (2019) All-dielectric radar absorbing array metamaterial based on silicon carbide/carbon foam material. J Alloy Compd 781:883–891
5. Xiao S, Mei H, Han D, Cheng L (2019) 3D printed SiC nanowire reinforced composites for broadband electromagnetic absorption. Ceram Int 45:11475–11483
6. Song W, Cao M, Fan L, Lu M, Li Y, Wang C, Ju H (2014) Highly ordered porous carbon/wax composites for effective electromagnetic attenuation and shielding. Carbon 77:130–142
7. Liu W, Tan S, Yang Z, Ji G (2018) Hollow graphite spheres embedded in porous amorphous carbon matrices as lightweight and low-frequency microwave absorbing material through modulating dielectric loss. Carbon 138:143–153
8. Singh J, Singh C, Kaur D, Narang SB, Joshi R, R. Mishra S, Jotania R, Ghimire M, C. Chauhan C, (2016) Tunable microwave absorption in Co-Al substituted M-type Ba-Sr hexagonal ferrite. Mater Des 110:749–761
9. Golchinvafa S, Masoudpanah SM, Jazirehpour M (2019) Magnetic and microwave absorption properties of FeCo/$CoFe_2O_4$ composite powders. J Alloy Compd 809:151–746
10. Cao MS, Cai YZ, He P, Shu JC, Cao WQ, Yuan J (2019) 2D MXenes: electromagnetic property for microwave absorption and electromagnetic interference shielding. Chem Eng J 359:1265–1302
11. Deng R, Chen B, Li H, Zhang K, Zhang T, Yu Y (2019) MXene/Co_3O_4 composite material: stable synthesis and its enhanced broadband microwave absorption. Appl Surf Sci 488:921–930
12. Peymanfar R, Norouzi F, Javanshir S (2019) Preparation and characterization of one-pot PANi/Fe/Fe_3O_4/Fe_2O_3 nanocomposite and investigation of its microwave, magnetic and optical performance. Synthetic Met 252:40–49
13. Ling A, Tan G, Man Q, Lou Y, Chen S, Gu X (2019) Broadband microwave absorbing materials based on MWCNTs' electromagnetic wave filtering effect. Compos B 171:214–221
14. Luo H, Zhang X, Huang S, Shan D, Deng L, He L (2019) Infrared emissivity and microwave transmission behavior of flaky aluminum functionalized pyramidal-frustum shaped periodic structure. Infrared Phys Technol 99:123–128
15. Duan Y, Xi Q, Liu W, Wang T, Magn J (2016) Broadband superior electromagnetic absorption of a discrete-structure microwave coating. J Magn Magn Mater 416:155–163
16. Qian Y, Wei H, Dong J, Du Y, Fang X, Zheng W, Sun Y, Jiang Z (2017) Fabrication of urchin-like ZnO-MXene nanocomposites for highperformance electromagnetic absorption. Ceram Int 43:10757–10762
17. Luo H, Chen F, Wang X, Dai W, Xiong Y, Yang J, Gong R (2019) A novel two-layer honeycomb sandwich structure absorber with highperformance microwave absorption. Compos A 119:1–7
18. Choi WH, Kim CG (2015) Broadband microwave-absorbing honeycomb structure with novel design concept. Compos B 83:14–20
19. Feng J, Zhang Y, Wang P, Fan H (2016) Oblique incidence performance of radar absorbing honeycombs. Compos B 99:465–471
20. Liu T, Xu Y, Zheng D, Zhou L, Li X, Liu L (2019) Fabrication and absorbing property of the tower-like absorber based on 3D printing process. Phys B 553:88–95
21. Shen L, Pang Y, Yan L, Shen Y, Xu Z, Qu S (2018) Broadband radar absorbing sandwich structures with enhanced mechanical properties. Results in Physics 11:253–258
22. YangL FH, Liu J, Ma J, Zheng Q (2013) Hybrid lattice-core sandwich composites designed for microwave absorption. Mater Des 50:863–871

23. Choi I, Kim JG, Seo IS, Lee DG (2012) Radar absorbing sandwich construction composed of CNT, PMI foam and carbon/epoxy composite. Compos Struct 94:3002–3008
24. Wanga Z, Zhoua C, Khaliulinb V, Shabalovb A (2018) An experimental study on the radar absorbing characteristics of folded core structures. Compos Struct 194:199–207
25. Zhou Q, Yin X, Ye F, Liu X, Cheng L, Zhang L (2017) A novel two-layer periodic stepped structure for effective broadband radar electromagnetic absorption. Mater Des 123:46–53
26. Huang H, Wang W, Cao T, Kuang J, Deng Y, Hua M, Xie W (2020) Broadband radar absorbing performance of corrugated structure. Compos Struct 253:112809
27. Huang H, Wang W, Hua M, Kuang J, Ma Y, Guo Z, Xie W (2020) Broadband radar absorbing characteristic based on periodic hollow truncated cone structure. Physica B: Physics of Condensed Matter 595:412368
28. Huang Y, Song W, Wang C, Xu Y, Wei W, Chen M, Tang L, Fang D (2018) Multi-scale design of electromagnetic composite metamaterials for broadband microwave absorption. Compos Sci Technol 162:206–214
29. Ozden K, Yucedag OM, Kocer H (2016) Metamaterial based broadband RF absorber at X-band. Int J Electron Commun 70:1062–1070
30. Hou C, Li T, Zhao T, Zhang W, Cheng Y (2012) Electromagnetic wave absorbing properties of carbon nanotubes doped rare metal/pure carbon nanotubes double-layer polymer composites. Mater Des 33:413–418